Journal of The Electrochemical Society, **157** (10) D523-D527 (2010)
0013-4651/2010/157(10)/D523/5/$28.00 © The Electrochemical Society

Electrodeposition of Cobalt Selenide Thin Films

Fangyang Liu,* Bo Wang, Yanqing Lai, Jie Li,,z Zhian Zhang, and Yexiang Liu**

School of Metallurgical Science and Engineering, Central South University, Changsha, Hunan 410083, China

Cobalt selenide thin films have been prepared onto tin oxide glass substrates by electrodeposition potentiostatically from an aqueous acid bath containing H_2SeO_3 and $Co(CH_3COO)_2$ at 50°C. The electrodeposition mechanism was investigated by cyclic voltammetry. The morphological, compositional, structural, and optical properties of the deposited films have been studied using scanning electron microscopy, energy-dispersive X-ray spectroscopy, X-ray diffraction, and optical absorption techniques, respectively. The formation of cobalt selenide was confirmed to proceed via an underpotential deposition mechanism. Se-rich CoSe thin films with compact and homogeneous morphology and hexagonal crystal structure were obtained at a deposition potential of −0.5 V vs saturated calomel electrode. The electrodeposited CoSe film exhibits an optical absorption coefficient of higher than 10^5 cm^{-1} and an optical bandgap of 1.53 ± 0.01 eV.
 [DOI: 10.1149/1.3468675]

Manuscript submitted March 2, 2010; revised manuscript received June 30, 2010. Published August 11, 2010.

Late transition-metal selenides have received considerable attention in the past few years due to their unusual structures and electronic properties.[1,2] These materials, in thin-film form, have found many applications such as in solar cells,[3] light emitting devices,[4] catalysts,[5] superionic conductor,[6] etc. Several methods have been attempted to prepare these selenides thin films: molecular beam epitaxy,[7] metallorganic chemical vapor deposition,[8] evaporation,[9] chemical bath deposition,[10] electrodeposition,[3,11] and spray pyrolysis.[12] Compared with the other methods, electrodeposition has numerous advantages[3,13] including (*i*) a low cost, high rate process involving very simple and inexpensive equipment; (*ii*) a large-area, continuous, multicomponent, low temperature deposition method; (*iii*) deposition of films on a variety of shapes and forms; and (*iv*) no use of toxic gases, effective material use, and minimum waste generation (solution can be recycled). Many attempts have been made for the electrodeposition of late transition-metal selenide thin films such as Ni_xSe,[11] Fe_xSe,[3,14] ZnSe,[15] and Cu_xSe.[16] However, the preparation of cobalt selenide by this effective, low cost technique has not been reported.

In this work, cobalt selenide thin films were prepared by electrodeposition from an aqueous solution. The results of the investigation of the deposition mechanism by cyclic voltammetry (CV), as well as film composition, morphology, structure, and optical properties, were presented.

Experimental

The electrochemical experiments, including CV and electrodeposition, were carried out in a three-electrode cell configuration with a SnO_2-coated glass substrate (20 Ω/□) as the working electrode, a purity graphite plate as the counter electrode, and a saturated calomel electrode (SCE) as a reference electrode. All potentials are reported with respect to this reference. All substrates were ultrasonically cleaned with acetone, rinsed with deionized water (18.2 MΩ cm^{-1}), and then subsequently dried. The electrolyte solution consisted of 2 mM H_2SeO_3, 2 mM $Co(CH_3COO)_2$, and 100 mM LiCl. The pH of the solution was adjusted to 2.0 using concentrated HCl. Residual oxygen in the bath was removed by bubbling N_2 for 20 min before each experiment. A Princeton Applied Research 2273A potentiostat was used for all electrochemical experiments. The cyclic voltammograms were measured at a scan rate of 10 mV/s and were first scanned in the negative direction. All experiments were performed in a stagnant bath at 50°C.

The chemical composition, surface morphology, and crystalline properties of the prepared films were characterized by an energy-dispersive X-ray spectroscope (EDS, EDAX-GENSIS60S), a scanning electron microscope (SEM, JSM-6360LV), and an X-ray diffractometer (XRD, Rigaku3014), respectively. The optical properties of the films were determined by a Shimadzu UV-2450 spectrophotometer.

Results and Discussion

Figure 1 shows the cyclic voltammograms for the SnO_2 electrode in the 100 mM LiCl, pH 2.0 solution in the presence of 2 mM $Co(CH_3COO)_2$ and that corresponding to the blank solution. For the blank solution, it is observed that there are one cathodic peak at about −0.76 V and one anodic peak at about −0.41 V, which can be assigned to a diffusion-limited reduction of protons and hydrogen oxidation (Eq. 1), respectively.[17,18] For the $Co(CH_3COO)_2$ solution, the appreciably negative shift of the cathodic peak, suggesting that hydrogen evolution is somewhat inhibited, may be due to the decrease in H^+ concentration near the cathode surface caused by competitive adsorption of Co^{2+} and H^+ ions. After this cathodic peak, there is a gradual increase in current with further shifting the potential negatively up to a particular potential (−0.82 V in our experiment) at which the current shows a much steeper increase abruptly than that in the blank solution. Therefore, this particular potential is considered as the deposition potential of cobalt according to Eq. 2.[19] At potentials equal to, or below this deposition potential, both deposition of cobalt and evolution of hydrogen occur simultaneously. Anodic branch of cyclic voltammogram can also provide information about the deposit formed. The anodic peak located at about

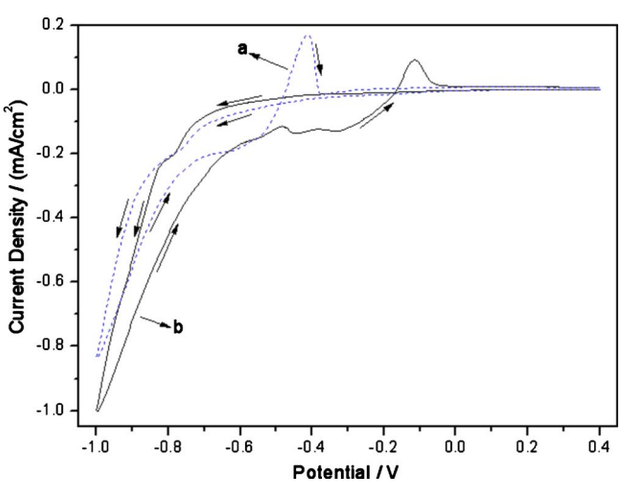

Figure 1. (Color online) Cyclic voltammograms for SnO_2 electrode at 10 mV/s scan rate and 50°C in 100 mM LiCl, pH 2.0 solution with (curve a) and without (curve b) 2 mM $Co(CH_3COO)_2$.

* Electrochemical Society Student Member.
** Electrochemical Society Active Member.
z E-mail: csulightmetals@126.com

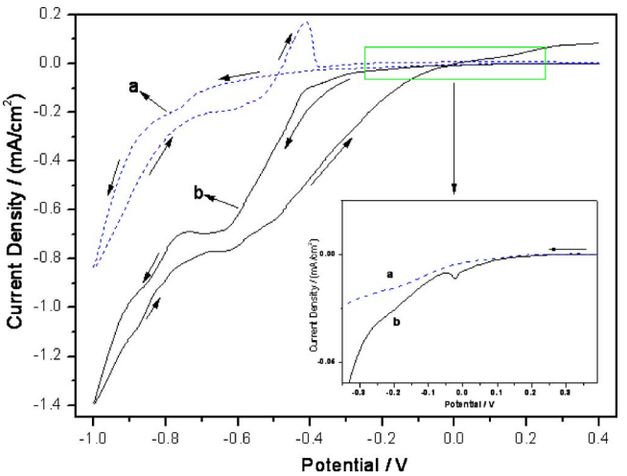

Figure 2. (Color online) Cyclic voltammograms for SnO_2 electrode at 10 mV/s scan rate and 50°C in 100 mM LiCl, pH 2.0 solution with (curve a) and without (curve b) 2 mM H_2SeO_3.

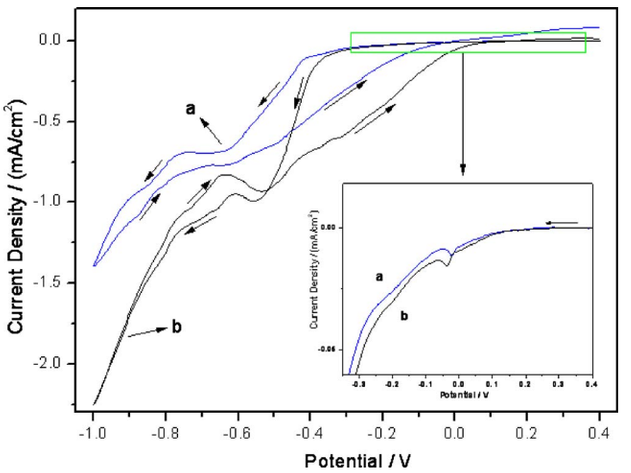

Figure 3. (Color online) Cyclic voltammograms for SnO_2 electrode at 10 mV/s scan rate and 50°C in 100 mM LiCl + 2 mM H_2SeO_3, pH 2.0 solution with (curve a) and without (curve b) 2 mM $Co(CH_3COO)_2$.

−0.48 V relates to hydrogen oxidation, as already shown in the cyclic voltammogram of the blank solution. Another anodic peak at −0.10 V with a shoulder at about −0.38 V, which has been frequently observed by others,[20-23] can be associated either with the dissolution of cobalt from the electrode to the solution in the form of different ionic species or with the dissolution of different cobalt phases, previously formed during the cathodic scan.[20,21,24] The current remains cathodic upon the sweep reversal, crossing over the current recorded during the negative sweep at −0.17 V. This current loop is attributed to the fact that the deposition of metals onto its own, in this case cobalt on cobalt, occurs at lower overpotentials than the deposition of metal onto different nature substrates, in this case cobalt on SnO_2 [25]

$$2H^+ + 2e \rightleftarrows H_2 \quad [1]$$

$$Co^{2+} + 2e \rightleftarrows Co \quad [2]$$

Figure 2 illustrates the cyclic voltammograms for the SnO_2 electrode in the 100 mM LiCl, pH 2.0 solution in the presence of 2 mM H_2SeO_3 and that corresponding to the blank solution. For the H_2SeO_3 solution, the curve displays two cathodic peaks at −0.36 and −0.65 V. In combination with previous studies,[26-32] the assignment of these two peaks is as follows: The weak cathodic peak at a potential of about −0.36 V corresponds to bulk selenium deposition through the four-electron reduction of Se(IV) to Se(0) proceeded by Eq. 3. Another cathodic peak at about −0.65 V corresponds to the six-electron reduction of Se(IV) to Se(−II) according to Eq. 4. The charge involved in the peak at −0.36 V is much smaller than that involved in the peak at −0.65 V, also contrasting with four-electron and six-electron processes, respectively. The product Se(−II) then undergoes a comproportionation reaction with Se(IV) in the solution (Eq. 5), leading to the chemical formation of Se(0).[29,32] This process of selenium deposition according to the reactions in Eq. 4 and 5 looks like the four-electron reduction (Eq. 3) when the concentration of H_2SeO_3 is high enough. It is also observed from the inset in Fig. 2 that there is an initial reductive feature before the peak at −0.36 V in the potential range from 0.15 to −0.05 V identified from a very weak reduction current, similar to that reported by other groups[31,32] and us.[33] This weak reduction current may correspond to the four-electron predeposition of selenium on SnO_2 substrate before the overpotential deposition of bulk selenium caused by the deposit–substrate interaction according to Eq. 3.[29-33] No anodic peaks are seen, although the anodic current is detected obviously because the potential is not positive enough for the development into an anodic peak for selenium oxidation.

$$H_2SeO_3 + 4H^+ + 4e^- \rightleftarrows Se + 3H_2O \quad [3]$$

$$H_2SeO_3 + 6H^+ + 6e^- \rightleftarrows H_2Se + 3H_2O \quad [4]$$

$$H_2SeO_3 + 2H_2Se \rightleftarrows Se + 3H_2O \quad [5]$$

Figure 3 presents the cyclic voltammograms for the SnO_2 electrode in the 100 mM LiCl + 2 mM $Co(CH_3COO)_2$ + 2 mM H_2SeO_3, pH 2.0 solution. Additionally, a voltammogram corresponding to the 100 mM LiCl + 2 mM H_2SeO_3, pH 2.0 solution is shown for comparison. The initial reductive feature beginning from 0.15 V and corresponding to the predeposition of selenium is observed again from the inset of Fig. 3. However, the current of this reductive feature in the binary Co–Se system is slightly larger than that in the unitary 2 mM H_2SeO_3 solution, and this increase in current continues to extend to the four-electron bulk Se deposition potential region. The small increase in current can be reasonably attributed to the contribution of additional reduction reaction with very slow deposition kinetics, which involves cobalt forming cobalt selenide proceeded by Eq. 6. The deposition of Co thus begins much earlier on a Se surface than on the SnO_2 surface. Whatever the cobalt selenide stoichiometry is, Co_xSe is presented here for simplicity. This is characteristic of the induced underpotential deposition mechanism, known as Kröger's mechanism,[34] which is caused by the large energy release in the formation of cobalt selenides. For instance, the value of the Gibbs free energy of the formation of CoSe is −40.74 kJ/mol [35] and, therefore, the redox potential of the reaction in Eq. 6 is shifted by an amount of $-\Delta G/2F = +0.211$ V theoretically with respect to the standard deposition potential of metallic cobalt. This mechanism has also been employed for the electrodeposition of many other compound semiconductors.[36-39] Obviously, the peak for the six-electron reduction reaction shows a significant positive shift, revealing that Co^{2+} helps in promoting the six-electron reduction of H_2SeO_3. This is because the generated H_2Se immediately reacts with Co^{2+} in the solution according to Eq. 7 due to the large free energy of formation of cobalt selenide again, which can facilitate the reaction in Eq. 4 in the forward direction.[40] By combining Eq. 4 and 7 to form Eq. 8, it is indicative once more that Co^{2+} promotes the six-electron reduction of H_2SeO_3. This positive shift leads to the overlapping of four-electron and six-electron Se(IV) reduction potential regions. Therefore, the much greater increase in current when the potential reaches about −0.35 V can be due to the contribution of two reduction reactions proceeded by Eq. 6 and 8 together. Moreover, the increase in current becomes more and more significant with further shifting the potential toward the

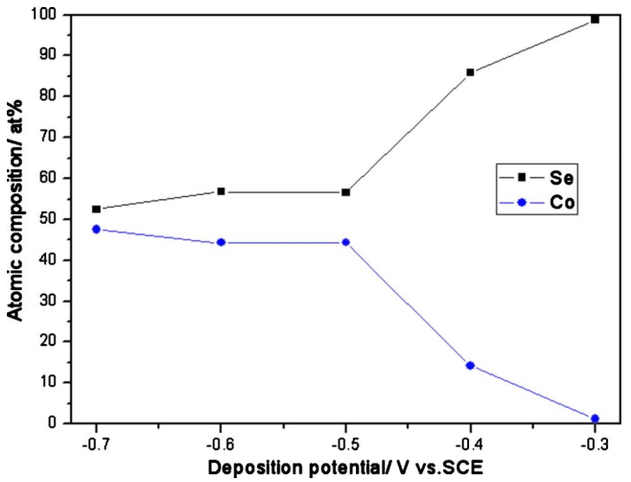

Figure 4. (Color online) The EDS composition of electrodeposited cobalt selenide films at 50°C and different potentials between −0.3 and −0.7 V from 2 mM $Co(CH_3COO)_2$ + 2 mM H_2SeO_3, pH 2.0 solution.

negative direction, which can be due to the growing reaction rates of both reactions in Eq. 6 and 8 under the enlarged reaction driving force with the negative shift of the cathodic potential

$$Se + xCo^{2+} + 2xe \rightleftarrows Co_xSe \quad [6]$$

$$H_2Se + xCo^{2+} \rightleftarrows Co_xSe + 2H^+ \quad [7]$$

$$H_2SeO_3 + xCo^{2+} + 4H^+ + (4 + 2x)e + \rightleftarrows Co_xSe + 3H_2O \quad [8]$$

All the above results allow us to conclude that the deposition of Co into the Co_xSe solid phase can proceed through two different routes: surface-induced reduction by Se and reaction with H_2Se. In any case, the underpotential deposition of cobalt as cobalt selenide is apparent.

Figure 4 shows the EDS composition of cobalt selenide films deposited at different potentials between −0.3 and −0.7 V from the 2 mM $Co(CH_3COO)_2$ + 2 mM H_2SeO_3, pH 2.0 solution. The films electrodeposited at potentials more negative than −0.7 V show many pinholes and poor adherence because of hydrogen evolution and have not been considered. For films deposited at −0.3 V or more positive potentials, the content of Co is very low, making it difficult to confirm the incorporation of Co into films by an EDS

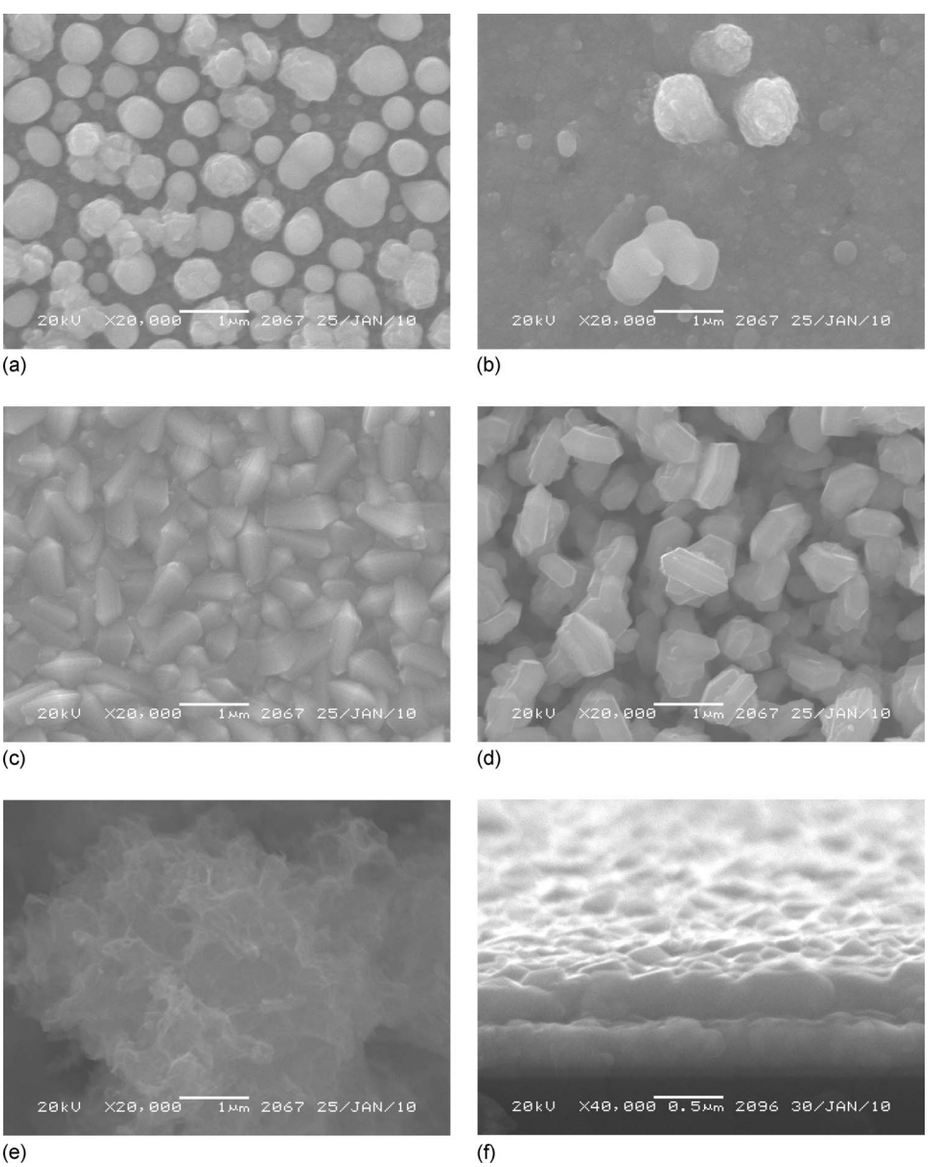

Figure 5. The SEM micrograph of electrodeposited cobalt selenide thin films at 50°C: (a) Deposition potential = −0.3 V, (b) deposition potential = −0.4 V, (c) deposition potential = −0.5 V, (d) deposition potential = −0.6 V, (e) deposition potential = −0.7 V, and (f) a cross-sectional view of cobalt selenide film electrodeposited at −0.5 V.

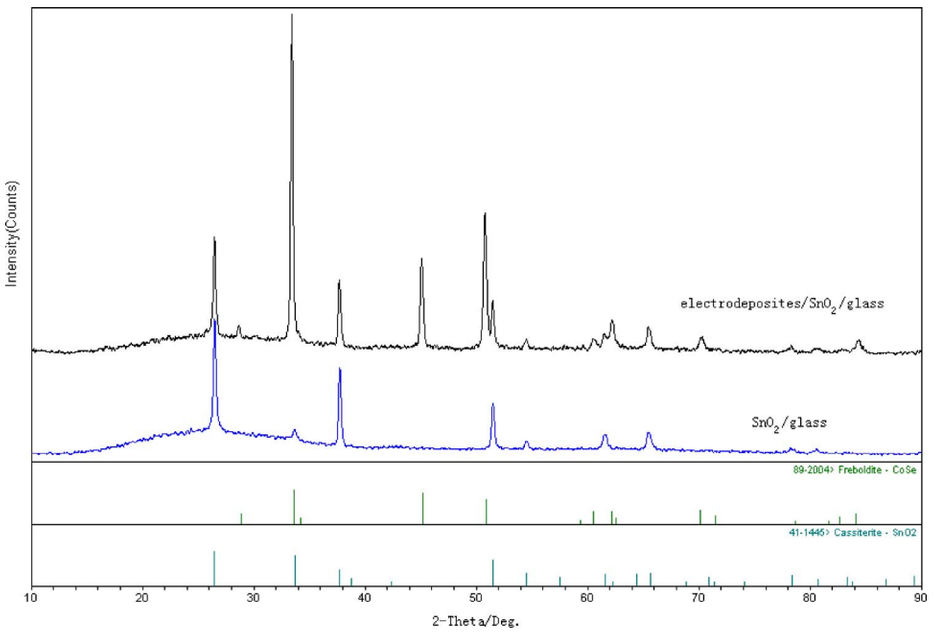

Figure 6. (Color online) X-ray diffraction pattern of cobalt selenide thin film electrodeposited at −0.5 V and 50°C on SnO_2 substrate.

(the EDS measurement error is within 3–5 atom %), which is attributed to the extremely slow kinetics of the underpotential deposition of cobalt selenide when the deposition potential is not negative enough based on the above CV studies. It is observed that, as the deposition potential shifts negatively, the cobalt content increases rapidly and the selenium content decreases in the film, leading to a composition of 56.6 atom % Se and 43.4 atom % Co obtained at −0.5 V. Further negative shift of the deposition potential, however, does not change the composition of the films significantly, which indicates that the electrodeposition process is mainly controlled by a diffusion independent of the deposition potential. This diffusion-controlled process has been maintained until the onset of the evolution of hydrogen, which disturbs the double layer forming on the electrode surface, leading to the instability of electrodeposition and accordingly film composition fluctuation.[41]

Figure 5a-e shows the dramatic difference of surface morphologies of electrodeposited Co–Se films at varied deposition potentials from −0.3 to −0.7 V. The film deposited at −0.3 V consists mainly of selenium and shows some clusters with sizes between 0.2 and 1 μm and some agglomerates with size larger than 2 μm (Fig. 5a). Similar morphologies of Se films were observed by Solaliendres et al.[42] The Se clusters are eliminated significantly with incorporation of a certain amount of Co with the deposition potential shifting negatively to −0.4 V (Fig. 5b). When the deposition potential reaches −0.5 V, the film shows a very compact and homogeneous surface morphology having isolated grains with uniform size and well-defined boundaries (Fig. 5c). With further negative shift of the deposition potential, the films became rough and porous (Fig. 5d) or even a loose structure with flocculent appearance (Fig. 5e). This is due to the high electrode reaction rate and excessive concentration polarization.[43]Generally, compact and smooth films are needed for application. Therefore, the deposition potential of −0.5 V was considered to be optimum for cobalt selenide thin-film electrodeposition. To get insight into the microstructure profile of the electrodeposited cobalt selenide thin film at −0.5 V, the cross-sectional SEM image is also present, as shown in Fig. 5f. The compact and uniform cobalt selenide thin film consisting of large grains extending from the bottom to the top of the film is obtained, and the thickness of the film is ~400 nm.

Figure 6 displays the XRD patterns measured for the electrodeposited cobalt selenide thin film at −0.5 V and the SnO_2/glass substrate. The results clearly indicate that all diffraction peaks, except the peaks of SnO_2 (JCPDS card no. 41-1445), which come from the substrate, perfectly match with the hexagonal phase of CoSe (JCPDS card no. 89-2004). No characteristic peaks were observed for other impurities. The excess Se according to the EDS composition cannot be indexed by an XRD due to its amorphous nature. Therefore, the deposits on the surface of the SnO_2 film consist of a compact film of the Se-rich CoSe sample.

Figure 7 shows the optical absorption coefficient (α) of the electrodeposited CoSe thin film as a function of photon energy ($h\nu$), converted from the transmission spectra recorded in the range of 300–900 nm. The sharp line near 300 nm (4.13 eV) is due to the change in source and the lower wavelength absorption by the substrate.[44] The absorption coefficient is larger than 10^{-5} cm^{-1} in the visible region, which supports the direct bandgap nature of the material[3] and reveals that the CoSe film can be considered to be a suitable material for photovoltaic solar energy conversion. Based on the allowed direct interband transition, the bandgap is determined to be 1.53 ± 0.01 eV by extrapolating the linear $(\alpha h\nu)^2$ vs $h\nu$ plots to

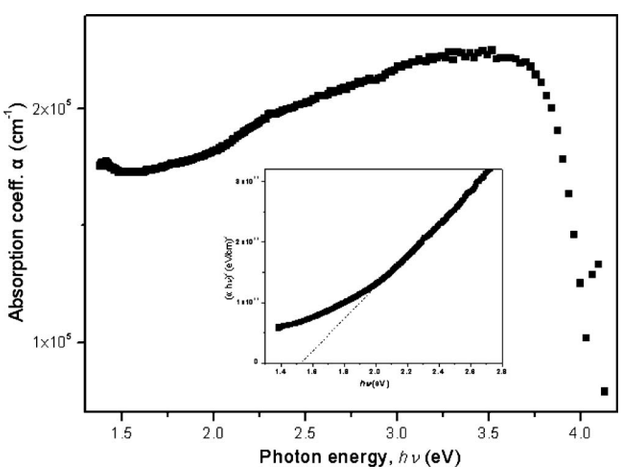

Figure 7. Optical absorption coefficient (α) of the electrodeposited CoSe thin film at −0.5 V and 50°C. The inset shows $(\alpha h\nu)^2$ vs $h\nu$ for CoSe film; the estimated bandgap is 1.52 eV.

$(\alpha h\nu)^2 = 0$, as depicted from the inset of Fig. 7. This value is quite close to the theoretical optimal value of light absorber for a single-junction solar cell.[45] These optical characteristics indicate that CoSe is a very promising material for thin-film solar cells.

Conclusions

Cobalt selenide thin films have been prepared onto tin oxide glass substrates by electrodeposition potentiostatically from an aqueous acid bath containing H_2SeO_3 and $Co(CH_3COO)_2$ at 50°C. The formation of cobalt selenide was inferred to proceed via an underpotential deposition mechanism from CV study, which may involve two routes: Co^{2+} reduction by a surface-induced effect from Se and/or reaction with H_2Se. Se-rich CoSe thin films with compact and homogeneous morphology, hexagonal crystal structure, and a direct optical bandgap of 1.53 ± 0.01 eV were obtained at a deposition potential of -0.5 V vs SCE.

Central South University assisted in meeting the publication costs of this article.

References

1. W. S. Sheldrick and M. Wachhold, *Angew. Chem., Int. Ed. Engl.*, **36**, 206 (1997).
2. W. Tremel, H. Kleinke, V. Derstroff, and C. Reisner, *J. Alloys Compd.*, **219**, 73 (1995).
3. S. M. Pawar, A. V. Moholkar, U. B. Suryavanshi, K. Y. Rajpure, and C. H. Bhosale, *Sol. Energy Mater. Sol. Cells*, **91**, 560 (2007).
4. I. M. Dharmadasa, A. P. Samantilleke, J. Young, M. H. Boyle, R. Bacewicz, and A. Wolska, *J. Mater. Sci.: Mater. Electron.*, **10**, 441 (1999).
5. Y. Feng, T. He, and N. Alonso-Vante, *Electrochim. Acta*, **54**, 5252 (2009).
6. S. Kashida and J. Akai, *J. Phys. C*, **21**, 5329 (1988).
7. Y. Takemura, H. Suto, N. Honda, K. Kakuno, and K. Saito, *J. Appl. Phys.*, **81**, 5177 (1997).
8. X. J. Wu, Z. Z. Zhang, J. Y. Zhang, Z. G. Ju, D. Z. Shen, B. H. Li, C. X. Shan, and Y. M. Lu, *J. Cryst. Growth*, **300**, 483 (2007).
9. N. Hamdadou, J. C. Bernède, and A. Khelil, *J. Cryst. Growth*, **241**, 313 (2002).
10. P. P. Hankare, B. V. Jadhav, K. M. Garadkar, P. A. Chate, I. S. Mulla, and S. D. Delekar, *J. Alloys Compd.*, **490**, 228 (2010).
11. Z. Zainal, N. Saravanan, and H. L. Mien, *J. Mater. Sci.: Mater. Electron.*, **16**, 111 (2005).
12. B. Ouertani, J. Ouerfelli, M. Saadoun, B. Bessaïs, H. Ezzaouia, and J. C. Bernède, *Sol. Energy Mater. Sol. Cells*, **87**, 501 (2005).
13. R. N. Bhattacharya and A. M. Fernandez, *Sol. Energy Mater. Sol. Cells*, **76**, 331 (2003).
14. S. Thanikaikarasan, T. Mahalingam, K. Sundaram, A. Kathalingam, Y. D. Kim, and T. Kim, *Vacuum*, **83**, 1066 (2009).
15. R. Kowalik, P. Żabiński, and K. Fitzner, *Electrochim. Acta*, **53**, 6184 (2008).
16. L. Thouin, S. Rouquette-Sanchez, and J. Vedel, *Electrochim. Acta*, **38**, 2387 (1993).
17. E. Gómez, R. Pollina, and E. Vallés, *J. Electroanal. Chem.*, **386**, 45 (1995).
18. R. Oriňáková, M. Strečková, L. Trnková, R. Rozik, and M. Gálová, *J. Electroanal. Chem.*, **594**, 152 (2006).
19. S. S. Abd El Rehim, M. A. M. Ibrahim, and M. M. Dankeria, *J. Appl. Electrochem.*, **32**, 1019 (2002).
20. A. B. Soto, E. M. Arce, M. Palomar-Pardavé, and I. González, *Electrochim. Acta*, **41**, 2647 (1996).
21. M. Palomar-Pardavé, I. González, A. B. Soto, and E. M. Arce, *J. Electroanal. Chem.*, **443**, 125 (1998).
22. D. Grujicic and B. Pesic, *Electrochim. Acta*, **49**, 4719 (2004).
23. L. H. Mendoza-Huizar, J. Robles, and M. Palomar-Pardavé, *J. Electrochem. Soc.*, **152**, C265 (2005).
24. C. H. Rios-Reyes, L. H. Mendoza-Huizar, and M. Rivera, *J. Solid State Electrochem.*, **14**, 659 (2010).
25. M. Palomar-Pardavé, B. R. Scharifker, E. M. Arce, and M. Romero-Romo, *Electrochim. Acta*, **50**, 4736 (2005).
26. R. W. Andrews and D. C. Johnson, *Anal. Chem.*, **47**, 294 (1975).
27. C. Wei, N. Myung, and K. Rajeshwar, *J. Electroanal. Chem.*, **375**, 109 (1994).
28. B. M. Huang, T. E. Lister, and J. L. Stickney, *Surf. Sci.*, **392**, 27 (1997).
29. M. Alanyalioglu, U. Demir, and C. Shannon, *J. Electroanal. Chem.*, **561**, 21 (2004).
30. M. C. Santos and S. A. S. Machado, *J. Electroanal. Chem.*, **567**, 203 (2004).
31. T. A. Sorenson, T. E. Lister, B. M. Huang, and J. L. Stickney, *J. Electrochem. Soc.*, **146**, 1019 (1999).
32. M. Kemell, H. Saloniemi, M. Ritala, and M. Leskela, *Electrochim. Acta*, **45**, 3737 (2000).
33. Y. Lai, F. Liu, J. Li, Z. Zhang, and Y. Liu, *J. Electroanal. Chem.*, **639**, 187 (2010).
34. F. A. Kröger, *J. Electrochem. Soc.*, **125**, 2028 (1978).
35. H. Jelinek and K. L. Komarek, *Monatsch. Chem.*, **105**, 689 (1974).
36. K. Rajeshwar, *Adv. Mater.*, **4**, 23 (1992).
37. H. Saloniemi, T. Kanniainen, M. Ritala, M. Leskelä, and R. Lappalainen, *J. Mater. Chem.*, **8**, 651 (1998).
38. D. Del Frari, S. Diliberto, N. Stein, C. Boulanger, and J.-M. Lecuire, *Thin Solid Films*, **483**, 44 (2005).
39. M. Kemell, M. Ritala, H. Saloniemi, M. Leskelä, T. Sajavaara, and E. Rauhala, *J. Electrochem. Soc.*, **147**, 1080 (2000).
40. P. W. Atkins, *Physical Chemistry*, 3rd ed., Oxford University Press, Oxford, UK (1985).
41. M. Paunovic and M. Schlesinger, *Fundamentals of Electrochemical Deposition*, Wiley-Interscience, Hoboken, New Jersey (1998).
42. M. O. Solaliendres, A. Manzoli, G. R. Salazar-Banda, K. I. B. Eguiluz, S. T. Tanimoto, and S. A. S. Machado, *J. Solid State Electrochem.*, **12**, 679 (2008).
43. Y. Lai, F. Liu, Z. Zhang, J. Liu, Y. Li, S. Kuang, J. Li, and Y. Liu, *Electrochim. Acta*, **54**, 3004 (2009).
44. R. Chandramohan, T. Mahalingam, J. P. Chu, and P. J. Sebastian, *Sol. Energy Mater. Sol. Cells*, **81**, 371 (2004).
45. S. C. Riha, B. A. Parkinson, and A. L. Prieto, *J. Am. Chem. Soc.*, **131**, 12054 (2009).